

Generating a non-perturbative mass gap using Feynman diagrams in an asymptotically free theory

Venkitesh Ayyar

Department of Physics, University of Colorado, Boulder, Colorado 80309, USA

Shailesh Chandrasekharan

Department of Physics, Box 90305, Duke University, Durham, North Carolina 27708, USA

Using the example of a two dimensional four-fermion lattice field theory we demonstrate that Feynman diagrams can generate a mass gap when massless fermions interact via a marginally relevant coupling. We introduce an infrared cutoff through the finite system size so that the perturbation series for the partition function and observables become convergent. We then use the Monte Carlo approach to sample sufficiently high orders of diagrams to expose the presence of a mass gap in the lattice model.

PACS numbers: 71.10.Fd, 02.70.Ss, 11.30.Rd, 05.30.Rt

I. INTRODUCTION

Understanding how a mass gap is generated in an asymptotically free theory like Yang-Mills theory continues to be a fascinating topic of research. Using Wilson's lattice formulation the origin of the mass gap is easy to derive within the strong coupling expansion [1]. Monte Carlo calculations have shown that the mass gap continues to exist and scales appropriately even for much weaker couplings. However, the challenge of course is to begin with a weak coupling expansion and show the presence of the mass gap. A Monte Carlo method that directly works within the weak coupling expansion could perhaps shed more light on the subject.

Recently, Monte Carlo methods have emerged that sample weak coupling Feynman diagrams in a variety of models [2–7]. Can such methods also be applicable to asymptotically free theories like Yang Mills theories and QCD? The obvious problem is that the weak coupling approach is an expansion in powers of the coupling g , while mass gaps in these theories arise non-perturbatively through an essential singularity of the form $M \sim e^{-\beta/g^2}$. So, at least naively, it seems impossible that weak coupling diagrams can be combined with Monte Carlo methods to generate a mass gap. As a first step in addressing this impasse, one can even ignore complications of a gauge theory and ask whether these weak coupling approaches can generate a mass gap in simpler two dimensional spin models that are known to be asymptotically free. This question was raised recently and partially addressed within the context of the two dimensional $O(N)$ and $U(N) \times U(N)$ model in the large N limit [8, 9]. The strategy that seems to work is to regulate the infrared divergences in a controllable way so as to make the weak coupling series convergent. A re-summation of the convergent series then exposes the existence of the mass gap.

In this work we use a similar strategy but consider a $SU(4)$ symmetric four-fermion model and thus explore the question of whether Feynman diagrams can generate a non-perturbative mass gap in asymptotically free theories without the simplifications that usually occur at large N [10, 11]. Two dimensional four-fermion field theories can be asymptotically free [12, 13], and can be formulated to have completely convergent weak coupling expansion by formulating them on a fi-

nite space-time lattice. However, in the absence of a small parameter like $1/N$ in large N models, the weak coupling diagrammatic series may converge only after summing over many terms. In our work we accomplish this summation using a Monte Carlo method and hence are able still expose the presence of a non-perturbative mass gap that is independent of the infrared regulator. By tuning the bare coupling to zero we can also explore the continuum limit. From a continuum quantum field theory perspective, there are connections of our approach to recent ideas of using resurgent functions and trans-series combined with boundary conditions that control infrared divergences to define the perturbation series non-perturbatively [14–16].

The physics of our lattice model is interesting from other perspectives as well. For example it was recently studied extensively in three and four dimensions [17–21] and contains a weak coupling massless fermion phase and a strong coupling massive fermion phase without any spontaneous symmetry breaking. In three dimensions one finds a second order phase transition that separates these two phases. This quantum critical point is exotic and may contain emergent gauge fields [22]. We believe this critical point moves to the origin in two dimensions, and thus the mass generation mechanism in our model is likely to be similar to the one discussed in [23]. However, the mass should still scale exponentially with the coupling as in any asymptotically free theory. We show this explicitly in our work.

II. LATTICE MODEL

Two dimensional lattice four-fermion models have been studied extensively using Monte Carlo methods in the past, but mostly within the Wilson fermion formulation [24–28]. The most efficient way to perform the calculations involve using the worldline representation [29, 30]. However, this representation is not helpful for understanding how weak coupling perturbation theory using Feynman diagrams can help to generate the non-perturbative mass gap in these models. A simple model that can be studied by sampling Feynman diagrams using a Monte Carlo method, is the reduced staggered fermion

model whose action is given by

$$S(\psi) = \frac{1}{2} \sum_{x,y,a} \psi_x^a M_{x,y} \psi_y^a - U \sum_x \psi_x^4 \psi_x^3 \psi_x^2 \psi_x^1. \quad (1)$$

where $M_{x,y}$ is the free staggered fermion matrix

$$M_{x,y} = \frac{1}{2} \sum_{\alpha} \eta_{\alpha,x} (\delta_{x+\hat{\alpha},y} - \delta_{x-\hat{\alpha},y}). \quad (2)$$

with the phase factors $\eta_{1,x} = 1$, $\eta_{2,x} = (-1)^{x_1}$. It is easy to verify that this model can be obtained by discretizing the continuum two dimensional model,

$$S_{\text{cont}} = \int d^2x \left\{ \sum_{a=1,2; i=1,2} \bar{\psi}_a^i(x) (\sigma_{\alpha})_{ij} \partial_{\alpha} \psi_a^j(x) - U \left(\psi_1^2(x) \psi_1^1(x) \psi_2^2(x) \psi_2^1(x) + \bar{\psi}_1^2(x) \bar{\psi}_1^1(x) \bar{\psi}_2^2(x) \bar{\psi}_2^1(x) \right) \right\}, \quad (3)$$

where σ_{α} are 2×2 Pauli matrices. Discretizing (3) naively on a space-time lattice and using the well known spin diagonalization transformation in order to reduce the fermion doubling [31, 32], we obtain (1).

Note that there are no $\bar{\psi}_x^a$ fields in the lattice action. In the reduced staggered formulation, one keeps only the minimal number of fermion fields per site and defines them as ψ_x^a on all sites. We can define the partition function of our model to be

$$Z = Z_0 \int [d\psi] e^{-S(\psi)} \quad (4)$$

where Z_0 is chosen so that $Z = 1$ in the free theory. The Grassmann integration measure $[d\psi]$ is a product of $d\psi_x^1 d\psi_x^2 d\psi_x^3 d\psi_x^4$ on every site x .

At $U = 0$ our lattice model describes $N_f = 4$ flavors of free massless (two-component) Dirac fermions in the continuum limit, which is reached by simply exploring physics at large length scales as compared to the lattice spacing. As a probe of the long distance physics we can take space-time to be a torus of side L (in lattice units) in each direction with anti-periodic boundary conditions. In two dimensions, a free fermion field is expected to have a mass dimension $[\psi_a^i] = 1/2$. In our approach this can be seen by the scaling of the fermion propagator $G_f(x, y) \sim 1/|x - y|$ for large separations. In Fig. 1 we plot the scaling of the propagator at a separation of $|x - y| = L/2$ along one of the directions, $R = G_f(0, L/2)$ as a function of L and find that $R \sim 1.67/L$. In the same figure we also show the scaling of the susceptibility

$$\chi_1 = \frac{1}{2Z} \int [d\psi] e^{-S} \sum_y \left\{ \psi_0^a \psi_0^b \psi_y^b \psi_y^a \right\}, \quad (5)$$

as a function of L and see the expected infrared divergence. This means the coupling U is marginal as expected from continuum perturbative power counting. We will see later that in fact U is marginally relevant since an exponentially small mass gap is generated in this model when $U > 0$. This is consistent with asymptotic freedom as predicted originally by Gross and Neveu [12].

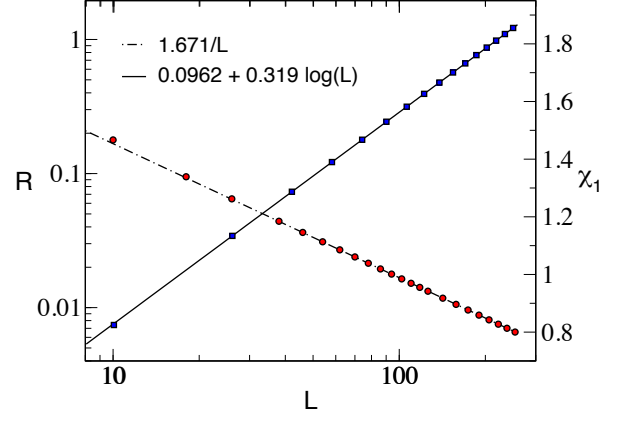


FIG. 1: The scaling of the fermion propagator at the mid point (R) and the susceptibility (χ_1) as a function of L in the free theory. This shows that the coupling U is perturbatively marginal as expected in the continuum.

III. THE PARTITION FUNCTION

The partition function of our model can be expanded in powers of the coupling

$$Z = \sum_k z_k U^k = \sum_k \left(\sum_{[x;k]} \Omega([x;k]) \right) U^k \quad (6)$$

where the coefficients z_k can be obtained as a sum over vertex configurations $[x;k] = \{x_1, x_2, \dots, x_k\}$ of an ordered set of k different lattice sites where the interactions occur. The weight of each vertex configuration is given by

$$\Omega([x;k]) = Z_0 \left(\int \left[\prod_x d\psi_x \right] e^{-\frac{1}{2} \sum_x \psi_x M_{x,y} \psi_y} \psi_{x_1} \psi_{x_2} \dots \psi_{x_k} \right)^4, \quad (7)$$

which is a sum over Feynman diagrams obtained through the regular Wick contractions. For each flavor the sum gives the Pfaffian of a $k \times k$ matrix $W([x;k])$, whose matrix elements are given by the free staggered fermion propagator $G_f(x_i, x_j)$ between the sites in $[x;k]$ [20]. Thus, we obtain

$$\Omega([x;k]) = \left(\text{Pf}(W([x;k])) \right)^4, \quad (8)$$

which is guaranteed to be positive. A Monte Carlo method can then be used to sample vertex configurations $[x;k]$ distributed according to the probability distribution

$$P_k(U, [x;k]) = \frac{U^k}{Z(U)} \left(\text{Pf}(W([x;k])) \right)^4. \quad (9)$$

Due to symmetries of the model the only non-zero weights involve an equal number of even and odd sites in $[x;k]$ which implies that only even values of k contribute to the expansion.

Interestingly, the expansion (6) in powers of U is finite and completely convergent on a finite lattice, since the maximum

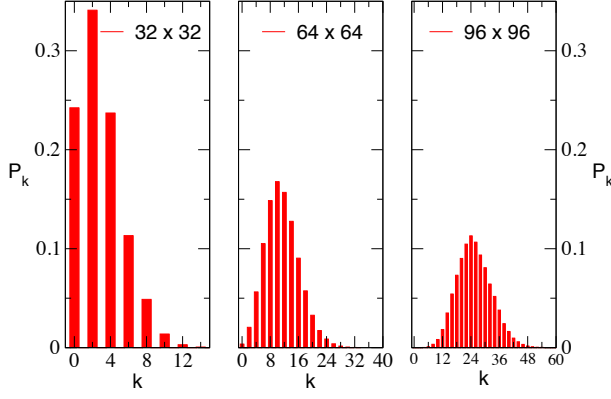


FIG. 2: Probability distribution of vertices in the partition function as a function of the lattice size at $U = 0.1$ for $L = 32, 64$ and 96 . The average density of vertices $\rho_k = \langle k \rangle / L^2 \approx 0.00267$ remains constant in all the three cases.

number of vertices that are allowed is L^2 . Our goal is to understand how the infrared divergences present in an asymptotically free theory manifest themselves in this convergent expansion. In order to gain some insight into the dominant terms in the expansion we define the probability distribution of vertices, $P_k(U) = z_k U^k / Z(U)$. Note that $P_k(U)$ as the sum over $P_k(U, [x, k])$ with a fixed k and U but different locations of the vertices. We can use Monte Carlo sampling to compute $P_k(U)$. In Fig. 2 we plot this probability distribution of vertices at $U = 0.1$ for different values of L . As we can see, sectors with large number of vertices are suppressed exponentially and the average number of vertices is much smaller than the maximum value $k_{\max} = L^2$. We discover that a more useful quantity is the average density of vertices $\rho(U) = \langle k \rangle / L^2$. In Fig. 3 we show how $\rho(U)$ changes with U . In the inset we plot this density at $U = 0.1$ for various lattice sizes and observe that it rapidly saturates in the thermodynamic limit. At $U = 0.1$, the average density is very small $\rho = 0.0027$.

It is easy to understand why the average density of vertices approaches a constant in the thermodynamic limit. From a statistical mechanics point of view one expects that the partition function scales as $Z = \exp(f(U)L^2)$ in the thermodynamic limit, where $f(U)$ is the free energy density. Since $f(U)$ is expected to be independent of the volume for sufficiently large volumes, the average density of vertices

$$\rho(U) = \frac{\langle k \rangle}{L^2} = (U/L^2)(\partial \ln Z(U)/\partial U) = U(\partial f(U)/\partial U), \quad (10)$$

is also independent of L . At a fixed L we can expand $f(U) = f_2 U^2 + f_4 U^4 + \dots$ and find connections between f_k 's and z_k 's. For example $f_2 = z_2/L^2$ and $f_4 = (z_4 - z_2^2/2)/L^2$ and so on. In Fig. 4 we plot f_2 and f_4 as functions of L for our model and see that both these coefficients are well behaved and do not show infrared divergences.

The connection between $Z(U)$ and $f(U)$ is well known in diagrammatic perturbation theory; the former contains con-

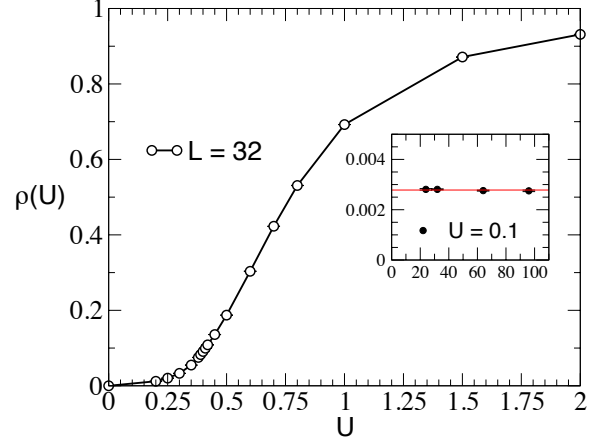


FIG. 3: Plot of the density of vertices $\rho(U)$ as a function of U . The inset shows the density at $U = 0.1$ as a function of L . We see that the density of vertices remains the same as L increases.

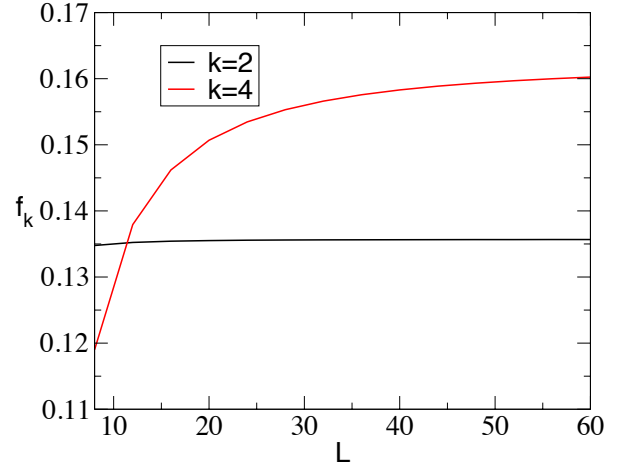


FIG. 4: Plot of the perturbative coefficients f_2 and f_4 in the expansion of the free energy as a function of L .

tributions from disconnected diagrams, while the latter gets contributions only from connected diagrams. If there are infrared divergences in perturbation theory they could appear in the f_k coefficients. From the discussion above we have shown that $Z(U)$ contains no infrared divergences except for the usual factors of the volume, but we cannot rule out such divergences in the expansion of $f(U)$, although in our model they do not appear in the first two terms f_2 and f_4 . This seems to be a feature of our current model due to its symmetries. Even if f_k 's contained divergences we can still extract $f(U)$ non-perturbatively through the integral

$$f(U) = \int_0^U \rho(U)/U. \quad (11)$$

However, we will need to compute $\rho(U)$ non-perturbatively by summing over the distribution of vertices generated by the Monte Carlo method. The usual infrared divergences in perturbation theory disappear once this resummation is performed.

IV. THE MASS GAP

In order to see how the diagrammatic method reproduces the mass gap we have studied two observables that are sensitive to the mass gap and both give very similar results [33]. Here we focus on one of them, which is the finite size susceptibility χ_1 defined in (5). As we already pointed out in Fig. 1, in the free theory χ_1 diverges logarithmically for large values of the lattice size L . However, if the mass gap M is generated we expect χ_1 will begin to level off roughly around $L \sim 1/M$. Further, the calculation of χ_1 can also be expressed as a sum over Feynman diagrams through the relation,

$$\chi_1 = \sum_{y,k} \left(\sum_{[x;k]} \Gamma_{0,y}([x;k]) P_k(U, [x;k]) \right) \quad (12)$$

where $\Gamma_{0,y}([x;k])$ is the ratio of two quantities: the numerator is the sum over all Feynman diagrams with two external sources located at the origin and at y in addition to the configuration of interaction vertices $[x;k] = \{x_1, x_2, \dots, x_k\}$ and the denominator is $\Omega([x;k])$, i.e., the sum over Feynman diagrams without the sources. This division makes $\Gamma_{0,y}([x;k])$ scale like a “connected” Feynman diagram for large volumes since a factor that scales exponentially in the volume is cancelled in the ratio. The configuration of interaction vertices $[x;k]$ is generated with probability $P_k(U, [x;k])$ and χ_1 is measured by choosing a lattice site at random which is defined as the origin and summing over all possible locations of y . If χ_1 contains infrared divergences, then it will increase indefinitely with L . We know that at $U = 0$ this does indeed occur as shown in Fig. 1. On the other hand, in our asymptotically free theory we expect a non-perturbative mass gap $M \sim \exp(-\beta/U)$ to be generated and χ_1 to level off when $L > 1/M$. In the left figure of Fig. 5 we plot χ_1 as a function of L at $U = 0.3$ and 0.4 . We observe that indeed χ_1 begins to level off around $L \sim 128$ at $U = 0.3$ and around $L \sim 32$ at $U = 0.4$. The fact that it takes a substantially larger lattice to level off at $U = 0.3$ as compared to $U = 0.4$ is an indication that M is decreasing rapidly. We also plot the $U = 0$ results for comparison.

Statistically speaking this implies that for most vertex configurations $[x;k]$ generated in the Monte Carlo sample, $\Gamma_{0,y}([x;k])$ begins to decay exponentially for points y far from the origin, although when y is close to the origin there is some enhancement when $U > 0$ as compared to $U = 0$ (see left figure of Fig. 5). It seems that the infrared divergence of the usual perturbation theory disappears for large lattices when we take into account a constant density of vertices. This means we need to consider large orders of perturbation theory. But what about the infrared divergences that clearly exist at small orders of perturbation theory? We believe these are the

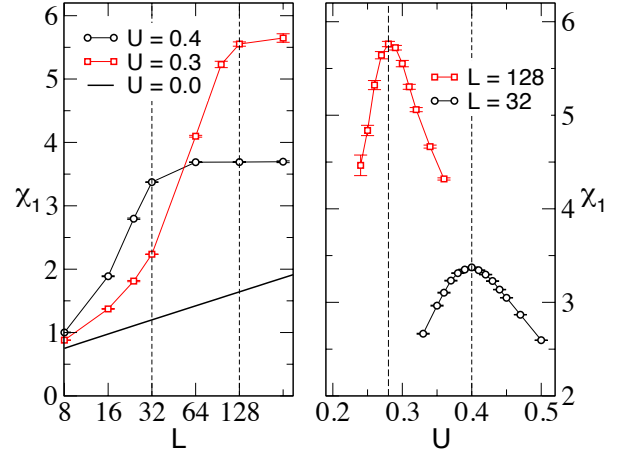


FIG. 5: Plot of the susceptibility χ_1 as a function of U for different lattice sizes. For value of L , we can define the mass scale $M'_b = 1/L$ that is generated when the location of the peak $U = U_p$ determines the scale $M'_b = 1/L$.

ones that cause the enhancement in χ_1 at small values of L but eventually, at large values of L , become statistically insignificant. In other words they are rare and hidden in the Monte Carlo fluctuations of the vertices that are generated. To see this, in Fig. 6 we plot the fluctuations in χ_1 during a sample of the Monte Carlo time history for $L = 64$ and $U = 0.4$. As can be seen from Fig. 5, for these parameters the theory has generated a mass gap with $\chi_1 \approx 3.7(5)$ being the saturated value of the susceptibility. However, as Fig. 6 shows there are still large but rare fluctuations in χ_1 that are three to four times larger than the average value. In perturbation theory the fact that these logarithmically divergent contributions are rare compared to finite contributions cannot be uncovered easily.

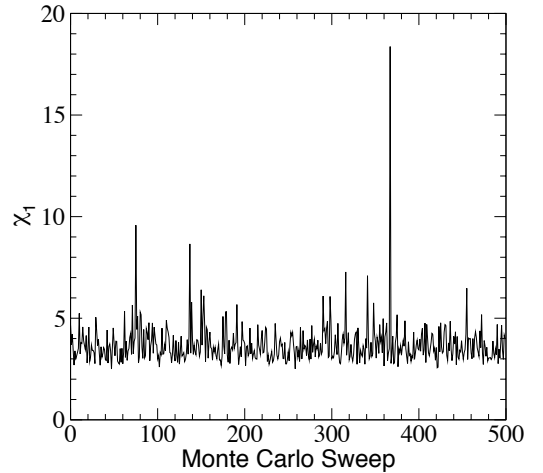


FIG. 6: Fluctuations of χ_1 in a sample of 500 vertex configurations generated consecutively during the Monte Carlo sampling.

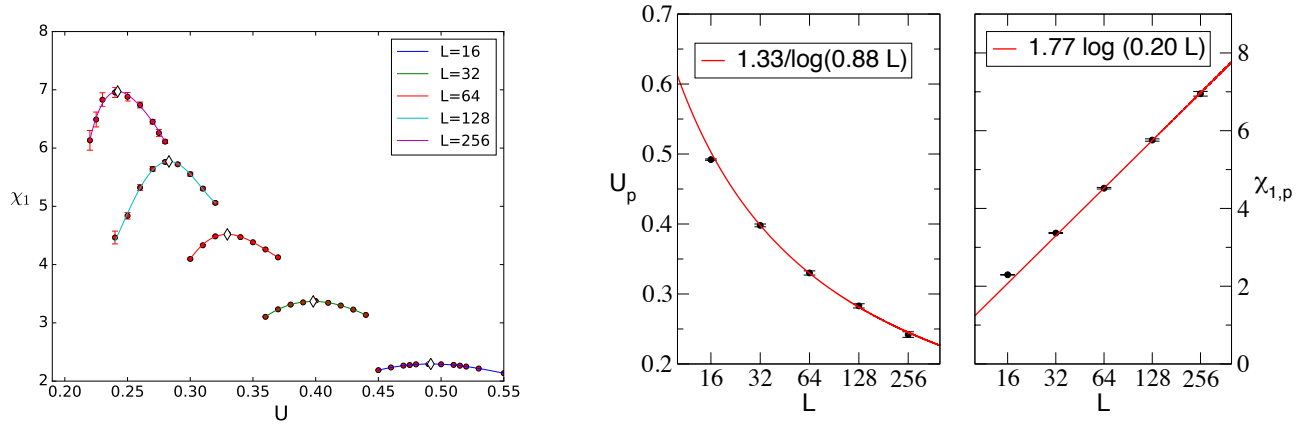


FIG. 7: (Left Figure) Plot of χ_1 as a function of U for different values of L . The locations of the peak obtained by fitting the data to a smooth curve are listed in Tab. I. (Right Figure) Plot of U_p and $\chi_{1,p}$ as a function of L and the fits to Eq.(13).

From the left plot of Fig. 5 we roughly expect $M \sim 1/32$ at $U = 0.4$ which decreases to $M \sim 1/128$ at $U = 0.3$. Using the exponential dependence of $\chi_1(L = \infty) - \chi_1(L)$ on L we can in principle extract M quantitatively. However, here we devise an alternate procedure and determine a slightly different mass scale M_b as follows. We first note that the susceptibility χ_1 has a peak as a function of U for every fixed value of L . This behavior is clearly visible in the right figure of Fig. 5 where we plot χ_1 as a function of U at $L = 32$ and 128 . For a fixed L if the peak occurs at $U = U_p$, we define a non-perturbative mass scale at U_p using the relation $M_b \equiv 1/L$. Comparing the left and right figures in Fig. 5 we see that our definition of M_b is also roughly consistent with the value of $1/L$ where χ_1 begins to level off. The locations of the peaks at various lattice sizes can be obtained rather accurately by fitting the data as shown in Fig. 7. Table I gives the values of the peak obtained through such a fit at different values of L .

L	$\chi_{1,p}$	U_p
16	2.293(2)	0.492(1)
32	3.368(5)	0.398(2)
64	4.520(20)	0.330(3)
128	5.760(30)	0.283(3)
256	6.950(60)	0.242(4)

TABLE I: Fit values for $\chi_{1,p}$ and U_p as a function of L .

If our theory is asymptotically free we expect that $M_b = \Lambda \exp(-\beta/U_p)$. Further, since $\chi_{1,p}$ is dimensionless it is expected to grow logarithmically in the continuum limit. Thus, for sufficiently large values of L we expect

$$\chi_{1,p} = \alpha \log(\Lambda_1 L), \quad U_p = \frac{\beta}{\log(\Lambda_2 L)}, \quad (13)$$

In Fig. 7 we show that our results are consistent with both

these expectations. The parameters obtained from the fit to our data gives $\alpha = 1.77(4)$, $\beta = 1.33(4)$, $\Lambda_1 = 0.20(1)$ and $\Lambda_2 = 0.88(9)$ [33]. While in principle the value of β can be matched to one loop perturbation theory, this can be very difficult and can require one to study extremely large correlation lengths [34]. Here we only study the qualitative exponential scaling of the mass gap, as was done long ago in lattice gauge theory but without using weak coupling expansion [35].

V. CONCLUSIONS

In this work we have shown how weak coupling Feynman diagrams can contain the information of a non-perturbative mass gap in an asymptotically free theory. Using a specific lattice model we first tamed the infrared divergences in the usual perturbation theory by formulating the problem in a finite volume. We then showed that the physics of the mass gap arises at sufficiently large volumes when we sample Feynman diagrams containing a finite density of interactions. The infrared divergences of the original perturbative expansion seem to be hidden in a few statistically insignificant vertex configurations. Our work suggests that a perturbative expansion organized in terms of Feynman diagrams containing a fixed density of interactions may be worth exploring. Exploring extensions of our work to gauge theories would also be interesting.

Acknowledgments

We thank T. Bhattacharya, S. Hands, R. Narayanan, U.-J. Wiese and U. Wolff for helpful discussions. The material presented here is based upon work supported by the U.S. Department of Energy, Office of Science, Nuclear Physics program under Award Number DE-FG02-05ER41368.

-
- [1] J. B. Kogut, *Rev. Mod. Phys.* **51**, 659 (1979).
 - [2] N. V. Prokof'ev and B. V. Svistunov, *Phys. Rev. Lett.* **81**, 2514 (1998).
 - [3] N. Prokof'ev and B. Svistunov, *Phys. Rev. Lett.* **99**, 250201 (2007).
 - [4] M. Boninsegni, N. V. Prokof'ev, and B. V. Svistunov, *Phys. Rev. E* **74**, 036701 (2006).
 - [5] N. V. Prokof'ev and B. V. Svistunov, *Phys. Rev. B* **77**, 125101 (2008).
 - [6] E. Kozik, K. Van Houcke, E. Gull, L. Pollet, N. Prokofev, B. Svistunov, and M. Troyer, *Europhys. Lett.* **90**, 10004 (2010).
 - [7] G. Cohen, E. Gull, D. R. Reichman, and A. J. Millis, *Phys. Rev. Lett.* **115**, 266802 (2015).
 - [8] P. V. Buividovich, *PoS LATTICE2015*, 293 (2016), 1510.06568.
 - [9] P. V. Buividovich and A. Davody (2017), 1705.03368.
 - [10] C. Kopper, J. Magnen, and V. Rivasseau, *Commun. Math. Phys.* **169**, 121 (1995).
 - [11] C. Kopper, *Commun. Math. Phys.* **202**, 89 (1999).
 - [12] D. J. Gross and A. Neveu, *Phys. Rev. D* **10**, 3235 (1974).
 - [13] E. Witten, *Nuclear Physics B* **145**, 110 (1978), ISSN 0550-3213.
 - [14] G. V. Dunne and M. Unsal, *JHEP* **11**, 170 (2012), 1210.2423.
 - [15] G. V. Dunne and M. Unsal, *Phys. Rev. D* **89**, 041701 (2014), 1306.4405.
 - [16] A. Cherman, D. Dorigoni, G. V. Dunne, and M. Unsal, *Phys. Rev. Lett.* **112**, 021601 (2014), 1308.0127.
 - [17] V. Ayyar and S. Chandrasekharan, *Phys. Rev. D* **93**, 081701 (2016).
 - [18] V. Ayyar and S. Chandrasekharan, *Phys. Rev. D* **91**, 065035 (2015).
 - [19] S. Catterall, *Journal of High Energy Physics* **2016**, 121 (2016).
 - [20] V. Ayyar and S. Chandrasekharan, *Journal of High Energy Physics* **2016**, 58 (2016), ISSN 1029-8479.
 - [21] S. Catterall and D. Schaich, *Phys. Rev. D* **96**, 034506 (2017).
 - [22] Y.-Z. You, Y.-C. He, C. Xu, and A. Vishwanath (2017), 1705.09313.
 - [23] Y. BenTov, *JHEP* **07**, 034 (2015), 1412.0154.
 - [24] K.-I. Nagai and K. Jansen, *Physics Letters B* **633**, 325 (2006), ISSN 0370-2693.
 - [25] C. Gattringer, V. Hermann, and M. Limmer, *Phys. Rev. D* **76**, 014503 (2007).
 - [26] W. Bietenholz, E. Focht, and U. J. Wiese, *Nucl. Phys.* **B436**, 385 (1995).
 - [27] I. Ichinose and K. Nagao, *Mod. Phys. Lett.* **A15**, 857 (2000).
 - [28] S. Aoki and K. Higashijima, *Prog. Theor. Phys.* **76**, 521 (1986).
 - [29] O. Bar, W. Rath, and U. Wolff, *Nucl. Phys.* **B822**, 408 (2009), 0905.4417.
 - [30] T. Korzec and U. Wolff, *PoS LAT2006*, 218 (2006), hep-lat/0609022.
 - [31] H. Sharatchandra, H. Thun, and P. Weisz, *Nucl. Phys.* **B192**, 205 (1981).
 - [32] C. van den Doel and J. Smit, *Nucl. Phys.* **B228**, 122 (1983).
 - [33] For further details about our work and analysis we refer the reader to the attached supplementary material.
 - [34] B. B. Beard, R. J. Birgeneau, M. Greven, and U.-J. Wiese, *Phys. Rev. Lett.* **80**, 1742 (1998).
 - [35] M. Creutz, *Phys. Rev. Lett.* **45**, 313 (1980).

Supplementary material

Here we document our Monte Carlo data and explain our analysis in greater detail.

Observables

In this work we measure three observables. They are the average monomer density ρ_m and the two bosonic susceptibilities χ_1 and χ_2 . Expressions for these are given below in Eqns.(A.14,A.15,A.16)

$$\rho_m = \frac{U}{L^2} \sum_x \langle \psi_x^4 \psi_x^3 \psi_x^2 \psi_x^1 \rangle \quad (\text{A.14})$$

$$\chi_1 = \frac{1}{2} \sum_x \langle \psi_0^1 \psi_0^2 \psi_x^1 \psi_x^2 \rangle \quad (\text{A.15})$$

$$\chi_2 = \frac{1}{2} \sum_x \langle \psi_0^1 \psi_0^2 \psi_x^3 \psi_x^4 \rangle \quad (\text{A.16})$$

Here averages are defined using the usual definition

$$\langle \mathcal{O} \rangle = \frac{1}{Z} \int [d\psi] \mathcal{O} e^{-S(\psi)} \quad (\text{A.17})$$

where Z is the partition function.

Testing the Monte Carlo Algorithm

In order to test our Monte Carlo results we have obtained exact analytic expressions for our observables on small lattices. We combine contributions of configurations with the same number of monomers into a single family labeled by k . Thus, we can write the partition function and the three observables defined above through expressions of the form

$$Z = 4^N \sum_{k=0}^N z_k (U/4)^k, \quad Z\rho_m = 4^N \sum_{k=0}^N a_{2k} (U/4)^k, \quad (Z/2)\chi_1 = 4^N \sum_{k=0}^N b_k (U/4)^k, \quad (Z/2)\chi_2 = 4^N \sum_{k=0}^{N-1} c_k (U/4)^k. \quad (\text{A.18})$$

In our model only those configurations which have an equal number of monomers on odd and even sites contribute to Z , ρ_m and χ_1 . Thus, $z_k = a_k = b_k = 0$ unless k is even. For χ_2 observable we must have one extra monomer on the even or odd site. This implies $c_k = 0$ unless k is odd. Expressions for these coefficients on square lattices of size $L = 4$ and $L = 6$ are given in Table II. We have tested our Monte Carlo algorithm against these exact results for a variety of couplings. In Table III we show the comparison of the Monte Carlo results with exact calculations. Overall the agreement is excellent and this gives us confidence that our sampling procedure is correct.

$L = 4$				
k	z_k	a_k	b_k	c_{k-1}
16	1	1	0	12
14	32	28	4	456
12	736	552	160	10896
10	13952	8720	4032	193632
8	240448	120224	78464	2789376
6	3571712	1339392	1255424	29884416
4	48234496	12058624	16515072	201326592
2	536870912	67108864	167772160	0
0	4294967296	0	1073741824	—

$L = 6$				
k	z_k	a_k	b_k	c_{k-1}
36	1.0×10^0	1.0×10^0	0	1.2×10^1
34	7.2×10^1	6.8×10^1	4.0×10^0	9.08×10^2
32	2.844×10^3	2.528×10^3	3.12×10^2	3.6956×10^4
30	7.9464×10^4	6.6220×10^4	1.3068×10^4	1.053340×10^6
28	1.740870×10^6	1.354010×10^6	3.82992×10^5	2.3353772×10^7
26	3.1613256×10^7	2.2831796×10^7	8.728764×10^6	4.25917988×10^8
24	4.93206108×10^8	3.28804072×10^8	1.63718040×10^8	6.615288804×10^9
22	6.779854296×10^9	4.143244292×10^9	2.618239172×10^9	$8.9563051092 \times 10^{10}$
20	$8.3706541569 \times 10^{10}$	$4.6503634205 \times 10^{10}$	$3.6573649104 \times 10^{10}$	$1.07405534638 \times 10^{12}$
18	$9.42203679280 \times 10^{11}$	$4.71101839640 \times 10^{11}$	$4.53974787568 \times 10^{11}$	$1.15306298447 \times 10^{13}$
16	$9.77835254141 \times 10^{12}$	$4.34593446285 \times 10^{12}$	$5.06840180904 \times 10^{12}$	$1.11456372088 \times 10^{14}$
14	$9.42271778661 \times 10^{13}$	$3.66439025035 \times 10^{13}$	$5.12909753014 \times 10^{13}$	$9.70247343789 \times 10^{14}$
12	$8.45677287995 \times 10^{14}$	$2.81892429332 \times 10^{14}$	$4.72023746127 \times 10^{14}$	$7.556401282 \times 10^{15}$
10	$7.05940382813 \times 10^{15}$	$1.96094550781 \times 10^{15}$	$3.9435513503 \times 10^{15}$	$5.17246103652 \times 10^{16}$
8	$5.45416462376 \times 10^{16}$	$1.21203658306 \times 10^{16}$	$2.96708502069 \times 10^{16}$	$2.99410799145 \times 10^{17}$
6	$3.85164352266 \times 10^{17}$	$6.4194058711 \times 10^{16}$	$1.97439045062 \times 10^{17}$	$1.3404915712 \times 10^{18}$
4	$2.4139636992 \times 10^{18}$	$2.682181888 \times 10^{17}$	$1.11848015872 \times 10^{18}$	3.641856×10^{18}
2	1.2321792×10^{19}	6.84544×10^{17}	4.9360128×10^{18}	0
0	4.096×10^{19}	0	1.3312×10^{19}	—

TABLE II: Coefficients in the expansion (A.18) for $L = 4$ and $L = 6$ lattices.

L	U	ρ_m		χ_1		χ_2	
		Exact	Monte-Carlo	Exact	Monte-Carlo	Exact	Monte-Carlo
4	0.1	252.1997×10^{-5}	$248(4) \times 10^{-5}$	$50250.3033 \times 10^{-5}$	$50244(4) \times 10^{-5}$	376.4032×10^{-4}	$369(6) \times 10^{-4}$
4	0.3	243.6685×10^{-4}	$244(1) \times 10^{-4}$	5226.738×10^{-4}	$5227(1) \times 10^{-4}$	1161.9073×10^{-4}	$1163(6) \times 10^{-4}$
4	0.5	783.7912×10^{-4}	$787(2) \times 10^{-4}$	5621.6117×10^{-4}	$5626(3) \times 10^{-4}$	2027.0147×10^{-4}	$2034(6) \times 10^{-4}$
4	1.0	5000.0×10^{-4}	$4996(6) \times 10^{-4}$	5499.6705×10^{-4}	$5503(1) \times 10^{-4}$	2999.6705×10^{-4}	$3006(3) \times 10^{-4}$
4	2.0	9216.2088×10^{-4}	$9215(2) \times 10^{-4}$	$14054.0293 \times 10^{-5}$	$14059(6) \times 10^{-5}$	506.7537×10^{-4}	$507(1) \times 10^{-4}$
4	20.0	$99937.3631 \times 10^{-5}$	$99933(2) \times 10^{-5}$	$125156.2985 \times 10^{-8}$	$125169(6) \times 10^{-8}$	46.9189×10^{-6}	$50(2) \times 10^{-6}$
6	0.1	271.345×10^{-5}	$272(4) \times 10^{-5}$	6573.4421×10^{-4}	$6577(2) \times 10^{-4}$	71.9009×10^{-3}	$72(1) \times 10^{-3}$
6	0.3	276.4455×10^{-4}	$276(1) \times 10^{-4}$	7210.1331×10^{-4}	$7211(5) \times 10^{-4}$	235.3032×10^{-3}	$235(1) \times 10^{-3}$
6	0.5	1022.8141×10^{-4}	$1024(3) \times 10^{-4}$	8686.679×10^{-4}	$8688(7) \times 10^{-4}$	459.9267×10^{-3}	$461(1) \times 10^{-3}$
6	1.0	6685.3777×10^{-4}	$6690(5) \times 10^{-4}$	6398.7824×10^{-4}	$6398(4) \times 10^{-4}$	4016.2128×10^{-4}	$4017(6) \times 10^{-4}$
6	2.0	9312.1586×10^{-4}	$9315(2) \times 10^{-4}$	$13637.6575 \times 10^{-5}$	$13633(5) \times 10^{-5}$	492.2129×10^{-4}	$490(1) \times 10^{-4}$
6	20.0	$99937.4317 \times 10^{-5}$	$99934(2) \times 10^{-5}$	125117.16×10^{-8}	$125124(4) \times 10^{-8}$	46.9018×10^{-6}	$49(1) \times 10^{-6}$

TABLE III: Comparison of our observables ρ_m , χ_1 and χ_2 , calculated using our Monte-Carlo algorithm against exact calculations on $L = 4$ and $L = 6$ lattices at various couplings.

U	L	ρ_m	χ_1	χ_2	U	L	ρ_m	χ_1	χ_2
0.100	128	0.0027770(82)	1.844(16)	0.604(16)	0.100	256	0.002773(14)	2.23(12)	0.93(18)
0.150	256	0.006477(23)	2.509(34)	1.373(50)	0.200	32	0.012034(17)	1.5099(17)	0.7047(21)
0.200	64	0.012131(13)	2.0513(69)	1.1665(68)	0.200	128	0.012194(23)	2.952(61)	1.995(53)
0.200	256	0.012204(33)	4.12(24)	3.20(21)	0.220	128	0.015255(29)	3.529(72)	2.640(67)
0.220	256	0.015457(34)	6.13(17)	5.24(16)	0.225	256	0.016410(22)	6.49(13)	5.62(11)
0.230	256	0.017393(28)	6.83(12)	6.02(11)	0.240	128	0.019086(48)	4.46(11)	3.63(10)
0.240	256	0.019471(38)	6.956(87)	6.197(75)	0.250	32	0.020324(24)	1.7789(27)	1.0479(29)
0.250	64	0.020712(22)	2.739(12)	1.964(12)	0.250	128	0.021318(37)	4.837(55)	4.056(51)
0.250	256	0.021866(38)	6.881(73)	6.153(53)	0.260	128	0.023946(51)	5.323(49)	4.590(54)
0.260	256	0.024463(26)	6.740(50)	6.041(37)	0.270	128	0.026845(43)	5.642(39)	4.933(35)
0.270	256	0.027249(31)	6.453(41)	5.756(29)	0.275	256	0.028837(45)	6.259(58)	5.596(42)
0.280	128	0.030126(48)	5.762(28)	5.098(23)	0.280	256	0.030406(40)	6.111(33)	5.459(22)
0.290	128	0.033624(41)	5.722(25)	5.069(17)	0.290	256	0.033851(49)	5.855(35)	5.212(24)
0.300	32	0.032967(41)	2.2361(43)	1.5843(45)	0.300	64	0.035580(51)	4.097(14)	3.447(14)
0.300	128	0.037380(63)	5.552(34)	4.916(23)	0.300	256	0.03765(11)	5.647(68)	5.030(47)
0.310	64	0.039875(54)	4.331(12)	3.714(12)	0.310	128	0.041590(67)	5.304(27)	4.707(19)
0.320	64	0.044699(60)	4.485(11)	3.895(10)	0.320	128	0.046032(65)	5.060(22)	4.490(16)
0.325	256	0.04851(10)	4.999(42)	4.421(29)	0.330	32	0.044573(60)	2.6648(52)	2.0622(53)
0.330	64	0.049793(60)	4.5276(95)	3.9557(78)	0.340	64	0.055166(60)	4.4714(84)	3.9259(64)
0.340	128	0.055868(86)	4.665(16)	4.122(11)	0.350	32	0.054811(78)	2.9649(53)	2.3973(55)
0.350	64	0.060984(61)	4.3834(80)	3.8506(57)	0.360	32	0.060820(86)	3.1037(52)	2.5534(52)
0.360	64	0.067013(63)	4.2600(71)	3.7430(52)	0.360	128	0.067305(89)	4.319(12)	3.8012(86)
0.370	32	0.067713(95)	3.2319(50)	2.6996(48)	0.370	64	0.073507(65)	4.1243(68)	3.6155(47)
0.380	32	0.07479(11)	3.3127(47)	2.7941(44)	0.380	64	0.080223(68)	3.9799(59)	3.4835(42)
0.380	128	0.08030(10)	3.9844(91)	3.4919(66)	0.390	32	0.08268(12)	3.3511(43)	2.8495(38)
0.390	64	0.087164(70)	3.8349(54)	3.3484(39)	0.400	32	0.09106(11)	3.3740(40)	2.8872(34)
0.400	64	0.094678(76)	3.6880(47)	3.2149(34)	0.400	128	0.09476(11)	3.6904(68)	3.2160(51)
0.400	256	0.09494(19)	3.695(14)	3.220(10)	0.410	32	0.09942(12)	3.3443(37)	2.8687(30)
0.420	32	0.10850(12)	3.2971(35)	2.8358(28)	0.430	16	0.09725(21)	2.0803(27)	1.6008(31)
0.430	32	0.11723(12)	3.2275(34)	2.7741(26)	0.440	32	0.12717(13)	3.1361(32)	2.6953(24)
0.450	16	0.11516(25)	2.1874(26)	1.7248(29)	0.450	32	0.13633(14)	3.0491(30)	2.6150(23)
0.450	64	0.137187(94)	3.0855(27)	2.6525(21)	0.460	16	0.12600(27)	2.2339(25)	1.7807(28)
0.470	16	0.13694(29)	2.2660(24)	1.8233(26)	0.470	32	0.15613(14)	2.8680(27)	2.4468(20)
0.475	16	0.14269(29)	2.2756(23)	1.8381(25)	0.480	16	0.14913(30)	2.2877(22)	1.8560(24)
0.490	16	0.16055(32)	2.2906(21)	1.8657(22)	0.500	16	0.17293(34)	2.2890(20)	1.8728(20)
0.500	32	0.18792(16)	2.5957(21)	2.1941(17)	0.500	64	0.18760(12)	2.6036(16)	2.2002(13)
0.500	128	0.18750(18)	2.6050(24)	2.2013(19)	0.510	16	0.18587(36)	2.2787(19)	1.8702(18)
0.515	16	0.19203(35)	2.2646(19)	1.8594(17)	0.520	16	0.19855(36)	2.2497(19)	1.8477(17)
0.530	16	0.21129(37)	2.2159(18)	1.8204(16)	0.550	16	0.23685(37)	2.1356(18)	1.7523(15)
0.550	64	0.24400(14)	2.2091(11)	1.83022(91)					

TABLE IV: Monte Carlo results for ρ_m , χ_1 and χ_2 for various values of U and L .

Monte Carlo Results

The results from our Monte-Carlo calculations are documented in Table IV. In order to analyze them we first plot the behavior of ρ_m as a function of the coupling U for various lattice sizes in Fig. 8. It increases from zero smoothly and even at $U = 0.3$ the density is small (less than 5 percent). Since ρ_m represents the density of vertices in the diagrammatic method, it is interesting to understand its finite size scaling. We see that the curves for lattices beyond $L = 32$ fall on top of each other implying that the relevant density of the vertices that play an important role in the physics is already correct at $L = 32$.

The behavior of the susceptibilities χ_1 and χ_2 as a function of the coupling U for various lattice sizes is shown in Fig. 9. In the main paper we focused on the susceptibility χ_1 . Here see that χ_2 also shows similar behavior. We note that both susceptibilities are roughly equal and show a peak as a function of U for each value of L . The location of the peaks can be used to define a non-perturbative mass gap. In Fig. 10 we plot these susceptibilities as a function of lattice size L for various couplings U .

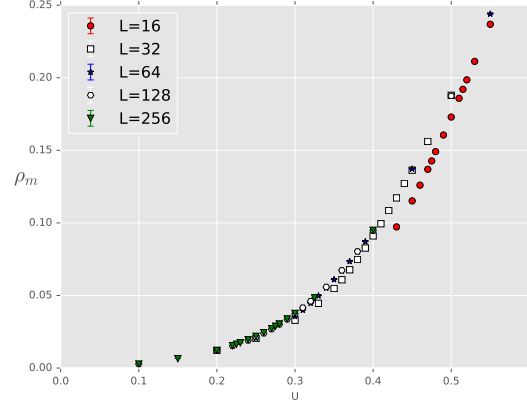


FIG. 8: Behavior of ρ_m as a function of the coupling U for the lattice sizes $L = 16, 32, 64, 128, 256$.

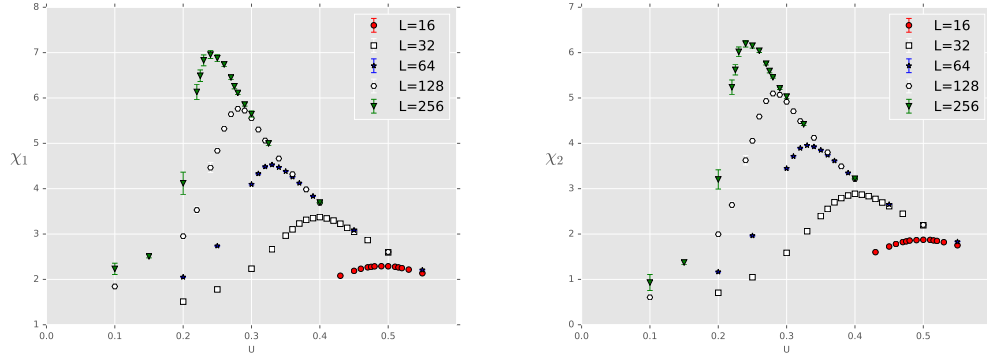


FIG. 9: Plot of the variation of the susceptibilities χ_1 χ_2 with coupling U for lattice sizes $L=16,32,64,128,256$. The location of the peak moves towards smaller values of U as L increases.

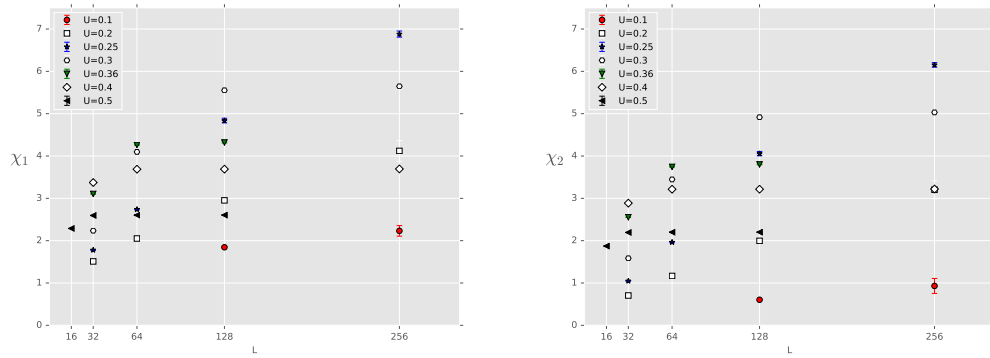


FIG. 10: Plot of the variation of the susceptibilities χ_1 χ_2 with lattice size L for various values of the coupling U . The susceptibilities rise initially but finally saturate at large L due to the formation of a mass gap.

Finite size scaling to locate the critical point

As we have seen above, both susceptibilities χ_1 and χ_2 show peaks for intermediate values of U at a fixed value of L . These peaks serve as pseudo-critical points that can be defined at a lattice size L . By performing a finite size scaling of how they change with lattice size one can extract the critical point of this theory. In our case we do know that the theory is asymptotically free and that the critical point is at the origin. This means we expect that

$$U_p = \frac{\beta}{\log(\Lambda L)}. \quad (\text{A.19})$$

Our goal is to verify this qualitatively. Thus, the first step is to estimate the value of U_p where the susceptibilities show a peak. Since the susceptibility is a maximum at this value of the coupling, we fit the susceptibilities near the peak to the form given by

$$\chi_{1,2} = a_0 + a_2 (U - U_p)^2 + a_3 (U - U_p)^3 + a_4 (U - U_p)^4 \quad (\text{A.20})$$

We performed a systematic analysis using three types of fits: a quadratic where a_3 and a_4 are fixed to zero, a cubic fit where a_4 is fixed to zero and a quartic fit where all parameters are allowed to vary. Tables V and VI show the results of systematic fits of χ_1 and χ_2 to the form given in Eqn. (A.20). Figures (11) and (12) show these fits pictorially. In Table VII we combine all these results and quote our best estimate for the fit values of χ_p and U_p . For the errors we sum of statistical and systematic errors from the various fits. Fig. (13) shows the quartic fits for all the lattice sizes.

L	Type of fit	Chi-sqr	χ_p	$\delta\chi_p$	U_p	δU_p	a_2	δa_2	a_3	δa_3	a_4	δa_4
16	quadratic	1.1114	2.2933	0.0013	0.4923	0.0005	-55.2534	3.5354	0.0000	0.0000	0.0000	0.0000
16	cubic	0.9770	2.2933	0.0011	0.4922	0.0006	-55.7011	1.8922	36.7719	75.6530	0.0000	0.0000
16	quartic	1.1835	2.2941	0.0012	0.4918	0.0005	-59.4665	2.7542	106.6690	45.6943	1897.4942	1222.0982
32	quadratic	2.3368	3.3681	0.0042	0.3988	0.0007	-160.1120	16.5230	0.0000	0.0000	0.0000	0.0000
32	cubic	1.1214	3.3677	0.0022	0.3980	0.0005	-158.0021	3.1383	632.6254	114.2130	0.0000	0.0000
32	quartic	1.3987	3.3679	0.0030	0.3980	0.0006	-158.8703	10.0483	625.0488	150.5280	580.5512	6295.2304
64	quadratic	3.8083	4.5195	0.0129	0.3311	0.0008	-398.7426	51.2187	0.0000	0.0000	0.0000	0.0000
64	cubic	1.1521	4.5178	0.0063	0.3293	0.0007	-389.7572	17.0960	3783.0246	737.6500	0.0000	0.0000
64	quartic	1.0774	4.5187	0.0064	0.3296	0.0007	-396.4272	21.9121	3422.7753	753.2829	10703.8631	23037.0197
128	quadratic	0.9618	5.7618	0.0167	0.2846	0.0005	-737.7290	37.1401	0.0000	0.0000	0.0000	0.0000
128	cubic	0.2793	5.7596	0.0093	0.2816	0.0005	-734.7338	24.0967	6693.0380	754.7323	0.0000	0.0000
128	quartic	0.3621	5.7707	0.0113	0.2830	0.0005	-860.8923	47.0663	3681.3421	477.4259	151223.4532	31909.8240
256	quadratic	0.1418	6.9355	0.0233	0.2421	0.0017	-620.3922	155.0111	0.0000	0.0000	0.0000	0.0000
256	cubic	0.2982	6.9670	0.0291	0.2438	0.0007	-1075.9692	100.6952	11689.5922	2632.9767	0.0000	0.0000
256	quartic	0.2462	6.9713	0.0279	0.2421	0.0013	-1101.4830	116.7963	21691.3719	8452.2653	-225021.7896	156882.5324

TABLE V: Table showing the systematic peak fits for χ_1

L	Type of fit	Chi-sqr	χ_p	$\delta\chi_p$	U_p	δU_p	a_2	δa_2	a_3	δa_3	a_4	δa_4
16	quadratic	2.4457	1.8737	0.0021	0.4989	0.0009	-55.4142	8.4233	0.0000	0.0000	0.0000	0.0000
16	cubic	1.6920	1.8737	0.0015	0.4994	0.0010	-57.5439	2.9933	11.4558	165.1145	0.0000	0.0000
16	quartic	1.6950	1.8746	0.0015	0.4988	0.0006	-62.2712	4.1086	125.2841	67.6321	3504.6035	2179.0863
32	quadratic	2.8621	2.8818	0.0035	0.4031	0.0006	-166.1171	10.1122	0.0000	0.0000	0.0000	0.0000
32	cubic	2.9150	2.8804	0.0033	0.4026	0.0010	-155.5164	6.4863	477.8623	405.6103	0.0000	0.0000
32	quartic	2.2587	2.8810	0.0032	0.4023	0.0006	-159.4701	11.4856	652.8482	134.1990	2825.6431	6870.9043
64	quadratic	1.9536	3.9498	0.0077	0.3325	0.0010	-327.2331	51.7558	0.0000	0.0000	0.0000	0.0000
64	cubic	0.9398	3.9511	0.0044	0.3319	0.0005	-376.0841	11.3091	3977.6380	553.2233	0.0000	0.0000
64	quartic	1.0265	3.9513	0.0049	0.3321	0.0005	-376.0437	18.9492	3706.3686	514.5751	1331.3217	18500.5385
128	quadratic	2.6373	5.0947	0.0207	0.2864	0.0007	-736.0865	49.9920	0.0000	0.0000	0.0000	0.0000
128	cubic	0.4076	5.0957	0.0087	0.2829	0.0005	-727.5055	23.2264	7660.0063	724.3519	0.0000	0.0000
128	quartic	0.5983	5.1037	0.0109	0.2843	0.0005	-843.3633	49.1091	5095.0906	509.9798	142339.5815	34343.3067
256	quadratic	0.2795	6.1841	0.0259	0.2450	0.0014	-647.3497	174.9559	0.0000	0.0000	0.0000	0.0000
256	cubic	0.4180	6.2207	0.0264	0.2453	0.0007	-1100.8041	90.8099	13474.7921	2443.9417	0.0000	0.0000
256	quartic	0.4420	6.2229	0.0283	0.2443	0.0014	-1096.8621	104.0742	19024.3513	7711.2843	-143899.3325	168588.6946

TABLE VI: Table showing the systematic peak fits for χ_2

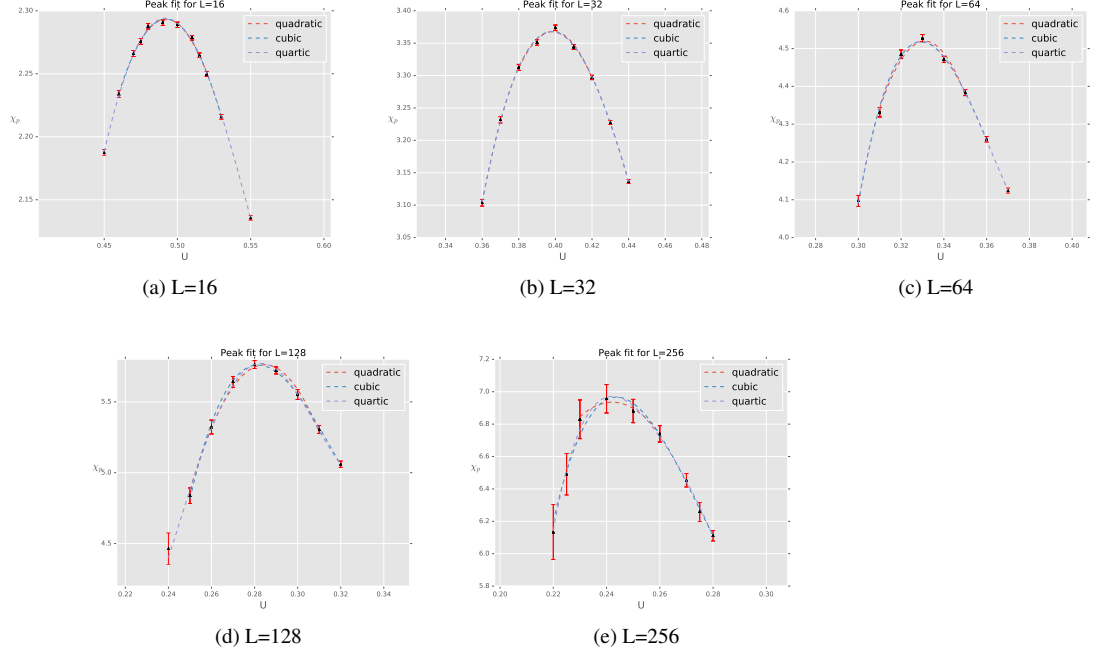


FIG. 11: Systematic fits for peak fits of χ_1 for $L=16, 32, 64, 128, 256$ respectively.

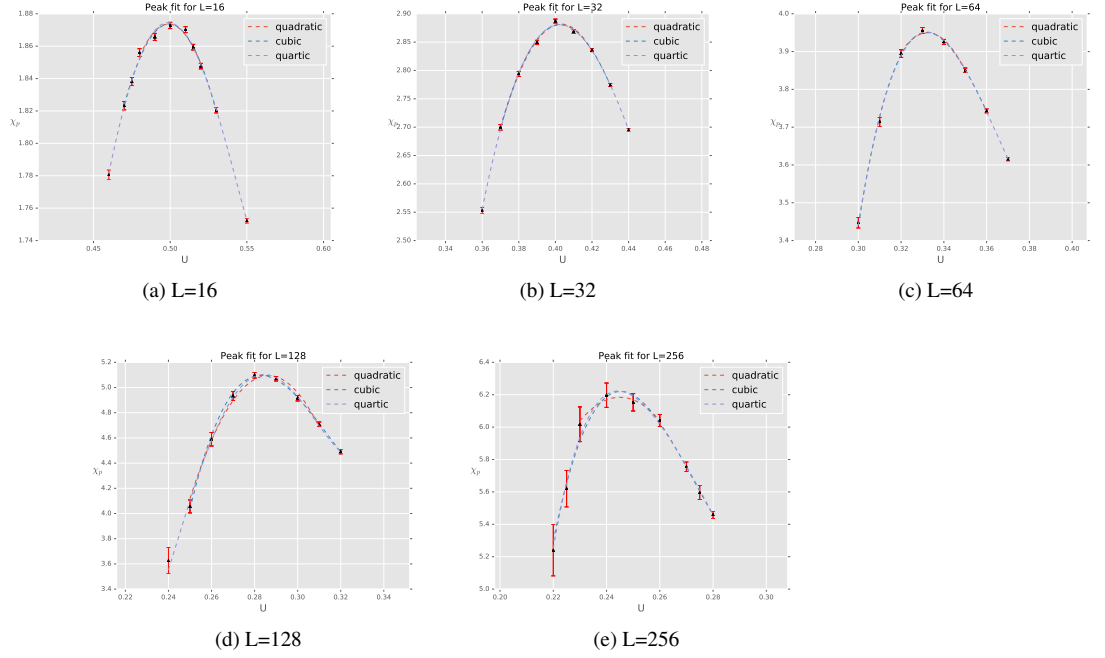


FIG. 12: Systematic fits for peak fits of χ_2 for $L=16, 32, 64, 128, 256$ respectively.

L	χ_{1p}	$\delta\chi_{1p}$	U_{1p}	δU_{1p}	L	χ_{2p}	$\delta\chi_{2p}$	U_{2p}	δU_{2p}
16	2.293	0.002	0.492	0.001	16	1.873	0.003	0.498	0.002
32	3.368	0.005	0.398	0.002	32	2.881	0.005	0.403	0.002
64	4.520	0.020	0.330	0.003	64	3.950	0.010	0.332	0.002
128	5.760	0.030	0.283	0.003	128	5.100	0.030	0.284	0.004
256	6.950	0.060	0.242	0.004	256	6.200	0.070	0.245	0.004

TABLE VII: Our estimates for χ_p and U_p for χ_1 and χ_2 . The errors quoted combines both statistical and systematic errors.

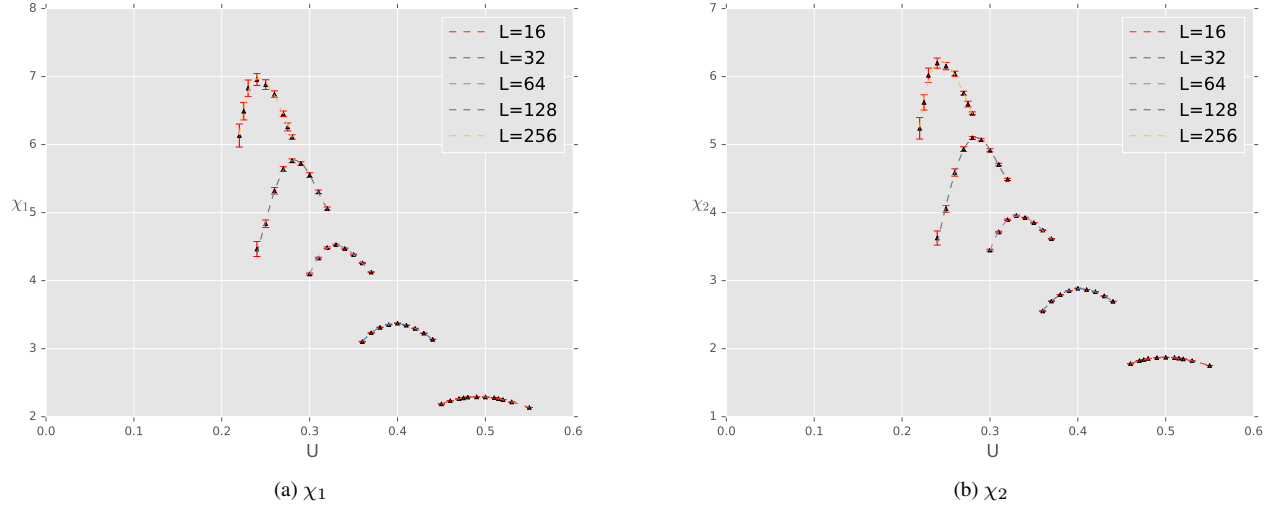


FIG. 13: Plot for quartic fits of χ_1 χ_2 for lattice sizes $L=16, 32, 64, 128, 256$. It is clear that the peak of curve shifts towards smaller U as lattice size increases.

Asymptotic Scaling

Having obtained the location of the peaks U_p as a function of L for each lattice size, we proceed to check the asymptotic scaling formula through the relation

$$U_p = \frac{\beta}{\log(\Lambda L)}, \quad (\text{A.21})$$

where λ is a mass scale in lattice units. We have performed a fit of our data to this form which should be valid for sufficiently large values of L . If we drop the data for the lattice $L = 16$, then for χ_1 we obtain $\beta = 1.33(4)$ and $\Lambda = 0.88(9)$ with a $\chi^2/\text{dof} = 0.5$. A similar fit for χ_2 gives $\beta = 1.31(4)$ and $\Lambda = 0.81(8)$ with a $\chi^2/\text{DOF} = 0.1$. These fits are shown in Fig. 14.

Due to asymptotic freedom $\chi_{1,p}$ and $\chi_{2,p}$ are expected to diverge logarithmically. At leading order we expect

$$\chi_p = \alpha \log(\Lambda' L) \quad (\text{A.22})$$

where Λ' is another mass scale in lattice units. For the fit of $\chi_{1,p}$ data we find $\alpha = 1.77(4)$ and $\Lambda' = 0.20(1)$ with a $\chi^2/\text{DOF} = 0.33$ while for the $\chi_{2,p}$ fit we find $\alpha = 1.64(4)$ and $\Lambda' = 0.17(1)$ with a $\chi^2/\text{DOF} = 0.30$. For these fits we had to drop both $L = 16$ and 32 data to obtain a good fit. These fits data are shown in Fig. 15.

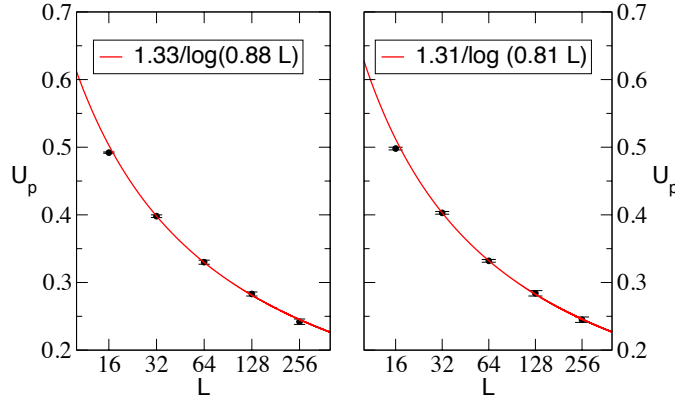


FIG. 14: Plots of U_p as a function of L and the fit to the form $U_p = \beta / \log(\Lambda L)$ as discussed in the text. The left plot uses χ_1 data while the right plot uses the χ_2 data.

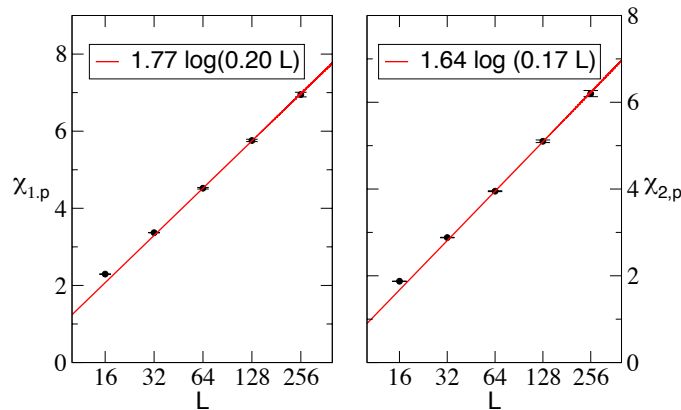


FIG. 15: Plots of $\chi_{1,p}$ and $\chi_{2,p}$ as a function of L and the fit to the form $\chi_p = \alpha \log(\Lambda' L)$ as discussed in the text.